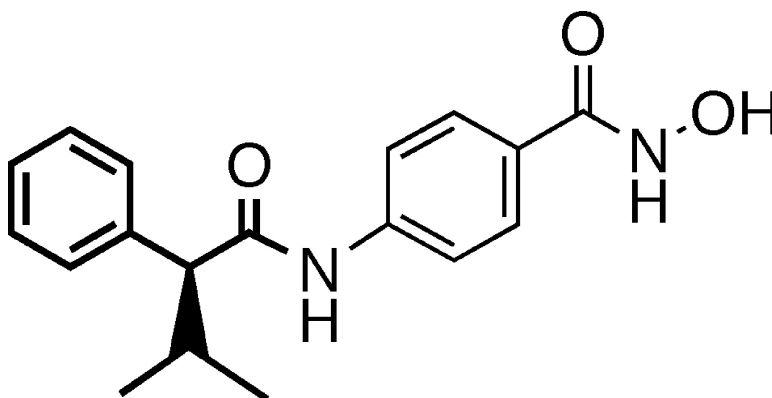# Journal of Medicinal Chemistry

## Article

# Structure-Based Optimization of Phenylbutyrate-Derived Histone Deacetylase Inhibitors

Qiang Lu, Da-Sheng Wang, Chang-Shi Chen, Yuan-Dong Hu, and Ching-Shih Chen

## More About This Article

Additional resources and features associated with this article are available within the HTML version:

- Supporting Information
- Links to the 4 articles that cite this article, as of the time of this article download
- Access to high resolution figures
- Links to articles and content related to this article
- Copyright permission to reproduce figures and/or text from this article

View the Full Text HTML

# Structure-Based Optimization of Phenylbutyrate-Derived Histone Deacetylase Inhibitors

Qiang Lu, Da-Sheng Wang, Chang-Shi Chen, Yuan-Dong Hu, and Ching-Shih Chen*

*Division of Medicinal Chemistry, College of Pharmacy, The Ohio State University, Columbus, Ohio 43210*

Previously, we developed a strategy to develop a novel class of histone deacetylase (HDAC) inhibitors by tethering short-chain fatty acids with $Zn^{2+}$-chelating motifs, which led to *N*-hydroxy-4-(4-phenylbutyryl-amino)benzamide (HTPB), a hydroxamate-tethered phenylbutyrate derivative with sub-micromolar potency in inhibiting HDAC activity and cancer cell proliferation. In this study, we carried out structure-based optimization of HTPB by using the framework generated by the structure of histone deacetylase-like protein (HDLP)−trichostatin A (TSA) complexes. Docking of HTPB into the HDLP binding domain suggested that the hydrophobic microenvironment encompassed by Phe-198 and Phe-200 could be exploited for structural optimization. This premise was corroborated by the greater potency of (*S*)-(+)-*N*-hydroxy-4-(3-methyl-2-phenylbutyrylamino)-benzamide [(*S*)-**11**] ($IC_{50}$ in HDAC inhibition, 16 nM), of which the isopropyl moiety was favorable in interacting with this hydrophobic motif. (*S*)-**11** at concentrations as low as 0.1 $\mu$M was effective in causing histone hyperacetylation and $p21^{WAF/CIP1}$ overexpression and suppressing proliferation in cancer cells.

## Introduction

Histone deacetylase (HDAC) is recognized as a promising target for cancer treatment because substantial evidence has linked the dysregulated histone code to the pathogenesis of many forms of cancer.[1,2] This premise is supported by the ability of HDAC inhibitors to trigger growth arrest, differentiation, and apoptosis in tumor cells through the transcriptional activation of a small set of genes that regulate cell proliferation and cell cycle progression.[3−9] These in vitro findings have also been confirmed in different xenograft tumor models, indicating the therapeutic relevance of HDAC inhibitors to cancer therapy. To date, several structurally distinct classes of HDAC inhibitors have advanced into phase I and/or phase II clinical trials in solid tumors and hematological malignancies, including short-chain fatty acids (e.g., valproate and phenylbutyrate), benzamide derivatives (e.g., MS-275), hydroxamic acids [e.g., suberyoyl anilide hydroxamic acid (SAHA) and LAQ824], and cyclic peptides (e.g., depsipeptide). However, because many of these agents are associated with low potency or cardiovascular toxicity, there is an urgency to develop novel HDAC inhibitors to overcome these problems.

Previously, Finnin et al. reported the three-dimensional structure of a histone deacetylase-like protein (HDLP), which provides insight into the unique mode of action of SAHA and trichostatin A (TSA) in HDAC inhibition.[10] The HDLP catalytic site consists of a narrow, tube-like pocket spanning the length equivalent to four- to six-carbon straight chains. A $Zn^{2+}$ cation is positioned near the bottom of this enzyme pocket, which, in cooperation with two His−Asp charge-relay systems, facilitates the deacetylation catalysis. Mechanistically, the long aliphatic chain of TSA and SAHA allows the

hydroxamate group to reach the polar bottom of the pocket and coordinate with the $Zn^{2+}$ cation, whereas the polar cap group at the other end of the spacer makes contact at the pocket entrance. On the basis of this three-component working model (i.e., cap group−linker−$Zn^{2+}$-chelating motif), we rationalized that the weak potency of short-chain fatty acids was, in part, attributable to their inability to access the $Zn^{2+}$ cation in the active-site pocket. Accordingly, we described a novel strategy of tethering short-chain fatty acids (valproate, butyrate, phenylacetate, and phenylbutyrate) with $Zn^{2+}$-chelating motifs through different aromatic amino acid linkers to develop a novel class of HDAC inhibitors.[11] Among a series of derivatives with varying potency, *N*-hydroxy-4-(4-phenylbutyryl-amino)benzamide (HTPB), a hydroxamate-tethered phenylbutyrate, represented an optimal agent with an $IC_{50}$ value of 44 nM, compared to 0.4 mM for the parent molecule phenylbutyrate.

In this study, we embarked on the structure-based optimization of HTPB by using the framework generated by the crystal structure of HDLP−TSA complexes. On the basis of the hypothesis that the hydrophobic residues flanking the cap group-binding motif could be exploited for lead optimization, we have generated (*S*)-**11**, an optically active α-branched phenylbutyryl derivative, with an $IC_{50}$ value of 16 nM in HDAC inhibition.

## Molecular Docking of HTPB

Despite distinct structural differences, HTPB and TSA displayed comparable potency in HDAC inhibition, suggesting a high degree of flexibility in ligand recognition within the HDAC catalytic domain. To compare the mode of protein−ligand interactions, TSA and HTPB were docked into the active-site pocket of HDLP following energy minimization (Figure 1).

We rationalized that the high potency of both HTPB and TSA was attributable to two structural features. A salt bridge formation between the hydroxamate and the zinc cation represents a major driving force for ligand

* To whom correspondence should be addressed. Address: Parks Hall, Rm 336, 500 West 12th Avenue, The Ohio State University, Columbus, OH 43210-1291. Tel: (614) 688-4008. Fax: (614) 688-8556. E-mail: chen.844@osu.edu.
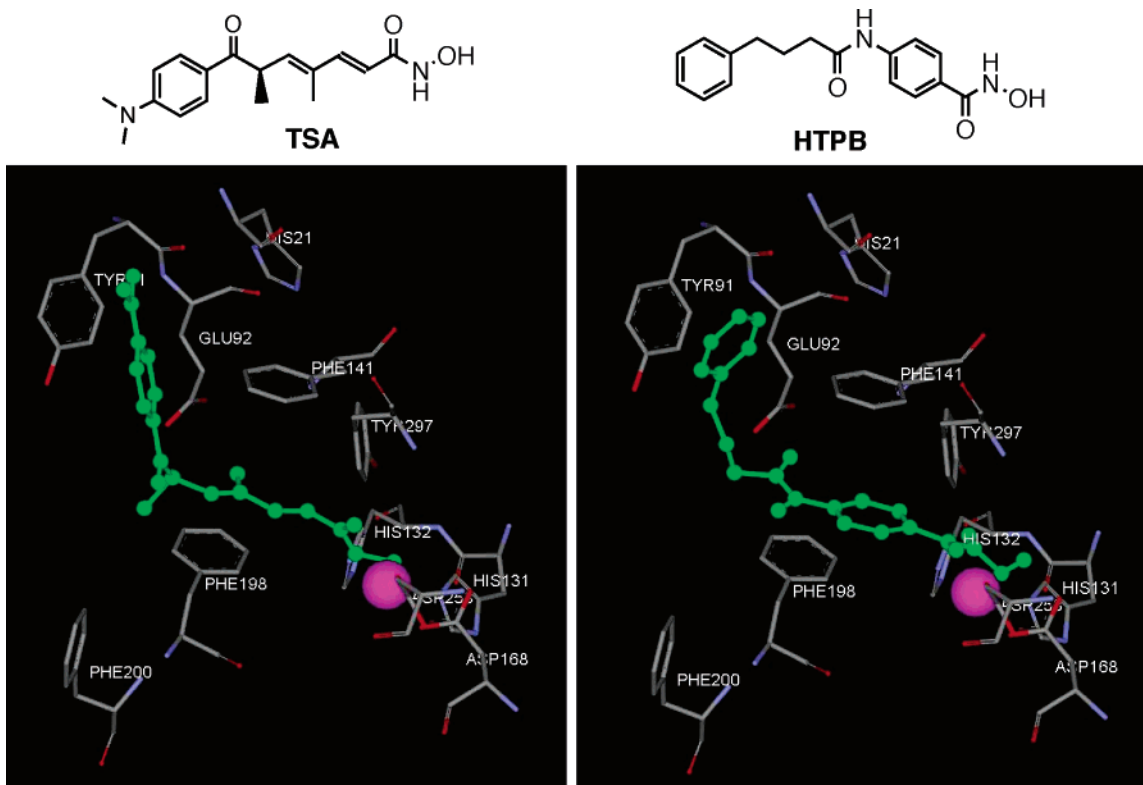
**Figure 1.** Modeled docking of TSA (left panel) and HTPB (right panel) into the active-site pocket of HDLP. Both small molecules are in green.

binding.[12] Equally important, the cap group and linker play a crucial role in anchoring the ligand inside the tube-like pocket through the hydrophobic and/or $\pi-\pi$ stacking interactions. As shown, a narrow, hydrophobic channel, generated by the two juxtaposed phenyl moieties of Phe-141 and Phe-198, was responsible for interacting with the linker, whereas the groove surrounded by Tyr-91 and Glu-92 was responsible for the cap group. Conceivably, the higher potency of TSA relative to HTPB ($IC_{50} = 5-15$ nM vs 44 nM, respectively) might, in part, be accounted for by hydrogen bonding between the dimethylamino moiety of TSA and the backbone amide.

## Chemistry

In light of the importance of $\pi-\pi$/hydrophobic interactions in ligand anchoring, disruption of any these interactions might lead to a decrease in inhibitory potency. To test this premise, we prepared compounds **1**–**6**, which represented hydroxamate-tethered derivatives of HTPB with varying chain lengths in the cap group/linker, and compound **7**, with an additional methyl function in the amide linkage of HTPB (Figure 2).

Moreover, we hypothesized that the hydrophobic microenvironment encompassed by Phe-198 and Phe-200 could be exploited to enhance the binding potency. Accordingly, we substituted the phenylbutyryl moiety of HTPB with different α-branched aromatic acyl groups (compounds **8**–**11**), of which the rationale was twofold. First, substitution at the α-position of the acyl cap group might enhance the metabolic stability by rendering the amide linkage more sterically hindered. Second, increasing the bulkiness of the acyl function might enhance binding affinity by augmenting the hydrophobic interactions with Phe-198 and Phe-200.
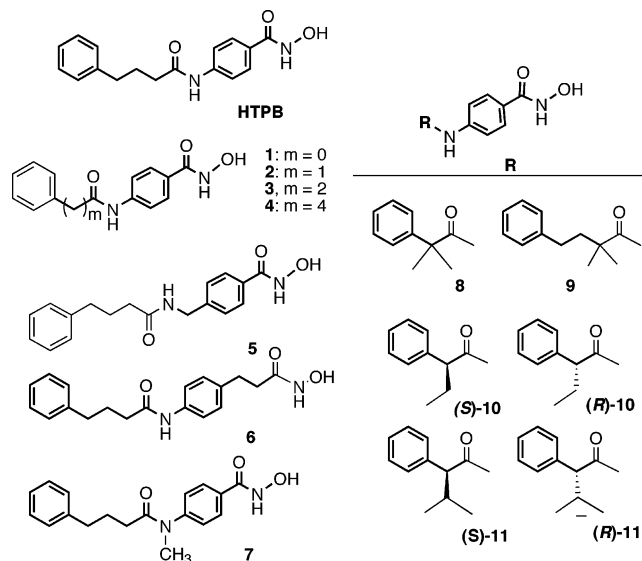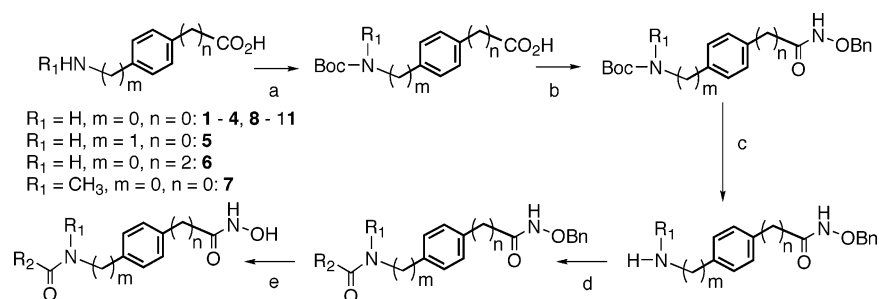


**Figure 2.** Structures of HTPB and compounds **1**–**11**.

These hydroxamate-tethered acyl conjugates were synthesized according to the procedure described in Scheme 1.

## Results

**Structural Basis for HDAC-Inhibitory Potency.** Altering the acyl cap group or the $\omega$-amino acid linker in HTPB resulted in a reduction in HDAC-inhibitory activity (Figure 3).

Among the five derivatives with varying acyl chain lengths, the relative potency was in the following order: HTPB (phenylbutyryl; $IC_{50} = 44 \pm 6$ nM) > **3** (phenylpropionyl; $IC_{50} = 110 \pm 37$ nM) > **2** (phenylacetyl; $IC_{50} = 157 \pm 26$ nM) > **1** (benzoyl; $IC_{50} = 210$

**Scheme 1.** General Synthetic Procedures for Compounds **1**−**11**[a]



R$_1$ = H, m = 0, n = 0: **1 - 4**, **8 - 11**
R$_1$ = H, m = 1, n = 0: **5**
R$_1$ = H, m = 0, n = 2: **6**
R$_1$ = CH$_3$, m = 0, n = 0: **7**

[a] Reagents: (a) (Boc)$_2$O, Et$_3$N, 1,4-dioxane, H$_2$O; (b) NH$_2$OBn·HCl, BOP−Cl, Et$_3$N; (c) TFA, CH$_2$Cl$_2$; (d) EDC, THF; and (e) 10% Pd/C, H$_2$, MeOH/THF.
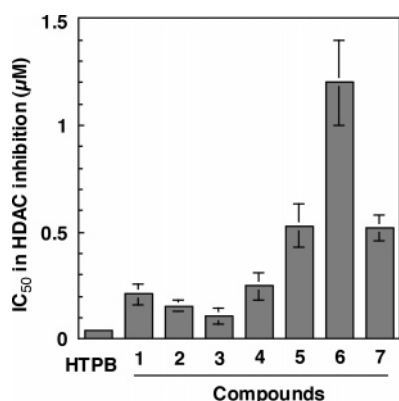


**Figure 3.** HDAC-inhibitory potency of compounds **1**−**7** compared to that of HTPB. In vitro HDAC assay was carried out using a commercial enzyme assay kit as described in Experimental Section. Data are presented as the means ± SD ($n = 3$).

nM ± 52 nM) > **4** (phenylpentanoyl; IC$_{50}$ = 250 ± 64 nM), indicating that the phenylbutyryl side chain af-

forded the optimal $\pi$−$\pi$ interactions with the Tyr-91 residue. Similarly, extending the $\omega$-amino acid linker, as in compounds **5** and **6**, caused an order of magnitude increase in IC$_{50}$ values (0.53 ± 0.10 $\mu$M and 1.2 ± 0.2 $\mu$M, respectively). Moreover, compound **7**, in which the amide proton of HTPB was substituted with a methyl function, exhibited a more than 10-fold decrease in potency (IC$_{50}$ = 0.52 ± 0.06 $\mu$M), which might be attributable to the steric hindrance imposed by the methyl group.

**Structural Optimization of HTPB: Steric and Stereochemical Effects.** To exploit the hydrophobic microdomain nearby Phe-198 and Phe-200 for structural optimization, we substituted the phenylbutyryl scaffold of HTPB with a series of $\alpha$-branched derivatives, including 2-methyl-2-phenylpropionyl (**8**), 2,2-dimethylphenylbutyryl (**9**), 2-phenylbutyryl (**10**), and 3-methyl-2-phenylbutyryl (**11**). It is noteworthy that except for compound **8**, these derivatives exhibited potency similar to or even higher than that of HTPB. The IC$_{50}$ values of these analogues in inhibiting HDAC activity were as
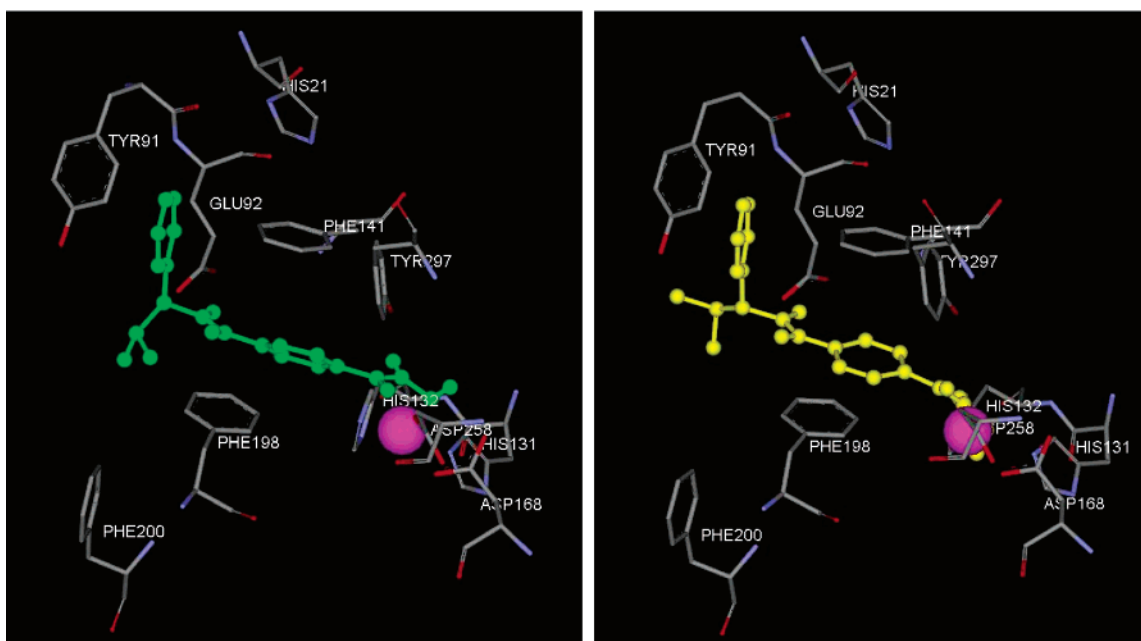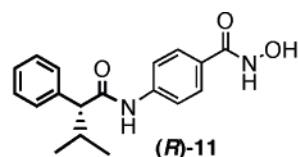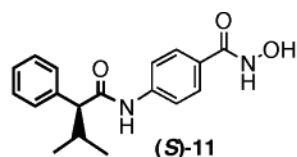


**Figure 4.** Modeled docking of (*S*)-**11** (left panel; in green) and (*R*)-**11** (right panel; in yellow) into the active-site pocket of HDLP.

follows: **8**, 98 ± 16 nM; **9**, 25 ± 6 nM; *rac*-**10**, 54 ± 13 nM; and *rac*-**11**, 30 ± 8 nM.

In light of the high potency of *rac*-**10** and *rac*-**11**, we further examined the activity of the optically active isomers of both agents to investigate the effect of stereo-chemistry on ligand binding. Our data indicated that stereoisomeric preference did exist in enzyme inhibition, that is, the potency of the (*S*) isomers of both compounds was significantly higher than that of their (*R*) counterparts. The $IC_{50}$ values were as follows: (*S*)-**10**, 34 ± 7 nM versus (*R*)-**10**, 68 ± 16 nM; (*S*)-**11**, 16 ± 4 nM versus (*R*)-**11**, 84 ± 21 nM. To shed light on this stereochemical discrimination, (*S*)- and (*R*)-**11** were docked into the binding motif after energy minimization (Figure 4).

This docking analysis revealed a major difference in the relative locality of the α-isopropyl group inside the pocket, which might account for the 5-fold difference in the respective HDAC-inhibitory potency. For (*S*)-**11**, the isopropyl moiety was located in the proximity of Phe-198 and Phe-200, which favored hydrophobic bonding with the phenyl rings. In contrast, the orientation of the isopropyl moiety of the (*R*) counterpart prohibited this hydrophobic interaction.

**Mechanistic Validation and Stereoselective Effect on Cell Viability.** As part of the target validation, we assessed the differential effects of these two enantiomers on the status of histone acetylation and the cyclin-dependent kinase inhibitor p21[WAF/CIP1] expression in DU-145 prostate cancer cells, which represent two important biomarkers associated with intracellular HDAC inhibition.[2] DU-145 cells were exposed to (*S*)- or (*R*)-**11** at 0.1, 0.25, 0.5, 1, and 2.5 μM in RPMI 1640 medium supplemented with 10% fetal bovine serum (FBS) for 48 h. Western blot analysis of the cell lysates indicated that (*S*)-**11** was effective in perturbing both biomarkers at concentrations as low as 0.1 μM, whereas (*R*)-**11** required a concentration of at least 0.5 μM to achieve an appreciable effect (Figure 5A). The preferential impact of (*S*)-**11** on these intracellular biomarkers also correlated with its higher efficacy in inhibiting the growth of DU-145 cells in 10% FBS-containing medium. The $IC_{50}$ values for (*S*)- and (*R*)-**11** were 0.11 ± 0.01 and 0.82 ± 0.13 μM, respectively, after a 96-h exposure (Figure 5B).

## Discussion

Previously, we described a strategy that tethered short-chain fatty acids with $Zn^{2+}$-chelating motifs to generate a novel class of HDAC inhibitors.[11] This effort has led to HTPB, an optimal agent with sub-micromolar potency in inhibiting HDAC activity and cancer cell proliferation. Because HTPB is structurally distinct from other potent HDAC inhibitors such as TSA and SAHA, we rationalized that a high degree of flexibility exists in the active-site pocket for accommodating cap groups with different stereoelectronic properties. On the basis of this premise, we carried out the structural optimization of HTPB by using the framework generated by the X-ray structure of HDLP−TSA complexes. Comparing the docking of HTPB versus TSA into the HDLP binding domain revealed unique structural features that underlie each molecule's ability to attain optimal inhibitory potency. For both molecules, hydrophobic and/or π−π interactions of its scaffold with the Phe-141/Phe-198 and Tyr-91/Glu-92 subdomains play an important role in anchoring the ligand to allow
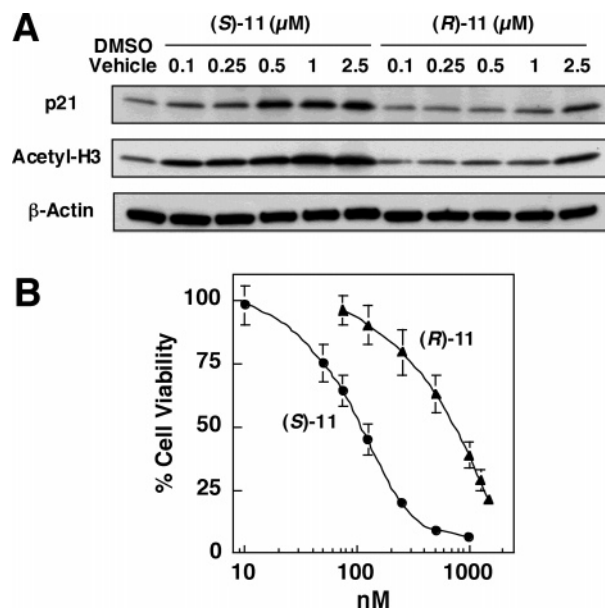


**Figure 5.** Cellular effects of (*S*)- and (*R*)-**11** in DU-145 prostate cancer cells. (A) Dose-dependent effect of (*S*)- and (*R*)-**11** on histone H3 acetylation and p21[WAF/CIP1] expression. DU-145 cells were exposed to (*S*)- or (*R*)-**11** at the indicated concentrations in 10% FBS-supplemented RPMI 1640 medium for 48 h. An equivalent amount of proteins from individual lysates was electrophoresed and probed by Western blotting with respective antibodies. Actin was used as an internal reference protein. (B) Dose-dependent effect of (*S*)- and (*R*)-**11** on cell viability. DU-145 cells were exposed to (*S*)- or (*R*)-**11** at the indicated concentrations in 10% FBS-supplemented RPMI 1640 medium for 96 h. Viable cells were examined by the MTT assay. Data are presented as the means ± SD (*n* = 6).

optimal access of the hydroxamate group to the zinc cation. Moreover, we proposed that the hydrophobic microenvironment encompassed by Phe-198 and Phe-200 could be exploited for enhancing the inhibitory potency. This premise was corroborated by the greater potency of the hydrophobic motif (*S*)-**11**, which displayed a favorable interaction with the α-isopropyl moiety. Moreover, the stereochemical preference of (*S*)-**11** over the (*R*) counterpart in HDAC inhibition is noteworthy. (*S*)-**11** at concentrations as low as 0.1 μM was effective in causing histone hyperacetylation and p21[WAF/CIP1] overexpression, whereas at least a 5-fold higher concentration was required to achieve the same effect for (*R*)-**11**. Conceivably, this stereoisomer strategy might also be applied to the optimization of other established HDAC inhibitors.

## Conclusion

Because many of the established HDAC inhibitors are associated with certain drawbacks, such as moderate potency or cardiotoxicity, there is an urgent need to develop novel agents for clinical testing. (*S*)-**11** provides a proof of concept that a high degree of flexibility exists in the active-site pocket to allow for the design of novel inhibitors with distinct stereoelectronic properties. In addition to high potency, simple chemical structure and oral bioavailability are among the unique features of this novel agent. Testing of the in vivo efficacy of this agent in a prostate tumor xenograft model is currently under way.

## Experimental Section

Chemical reagents and organic solvents were purchased from Aldrich unless otherwise mentioned. Nuclear magnetic

resonance spectra ($^1$H NMR) were measured on a Bruker 250 MHz. Chemical shifts ($\delta$) were reported in parts per million (ppm) relative to the TMS peak. Electrospray ionization (ESI) mass spectrometry analyses were performed with a 3-Tesla Finnigan FTMS-2000 Fourier Transform mass spectrometer. Elemental analyses were within ± 0.4% of calculated values. Flash column chromatography was performed with silica gel (230−400 mesh). Rabbit anti-acetyl-histone H3 polyclonal antibodies were purchased from Upstate Biotechnology (Lake Placid, NY), Rabbit anti-p21$^{WAF/CIP1}$ antibodies were obtained from Santa Cruz Biotechnology (Santa Cruz, CA). Mouse monoclonal anti-actin was from ICN Biomedicals (Irvine, CA). HRP-conjugated goat anti-rabbit IgG and HRP-conjugated goat anti-mouse IgG were obtained from Jackson ImmunoResearch (West Grove, PA).

Compounds **1**−**11** were synthesized according to the five-step procedure described in Scheme 1, the general methods of which are described as follows.

**Method a** [*tert*-butyl carbonate (*t*Boc-) protection]. Triethylamine (TEA, 1.5 equiv) was added to a solution of individual $\omega$-amino acids in aqueous dioxane (1:1), followed by the addition of di-*tert*-butyl dicarbonate (1.5 equiv). After being stirred overnight, solvents were removed under vacuum, and 3 N aqueous hydrochloric acid (4.5 equiv) was added dropwise to the residue. The resulting precipitate was collected, washed with water, and dried.

**Method b** [bis(2-oxo-3-oxazolidinyl)phosphoramidic chloride (BOP−Cl) coupling]. TEA (1 equiv) was added to a solution of the resulting acid in dry THF (5−10 mmol/mL) under N$_2$. The mixture was stirred for 10 min, and BOP−Cl (1.1 equiv), O-benzylhydroxylamine hydrochloride (1 equiv), and TEA (3 equiv) were added. After being stirred overnight, the solution was concentrated under vacuum, and ethyl acetate (100 mL) was added, followed by the addition of 3% NaHCO$_3$ (50 mL). The organic phase was separated, washed consecutively with water and saturated brine (50 mL each), dried over Na$_2$SO$_4$, and concentrated under vacuum. The resulting residue was purified by silica gel flash chromatography.

**Method c** (*t*Boc-deprotection). A solution of the above product (1 g) in a mixture of dichloromethane and trifluoroacetic acid (6:1, 35 mL) was stirred for 2 h. The solvent was evaporated under vacuum, and the residue was dissolved in ethyl acetate (100 mL). The mixture was washed consecutively with 50 mL of water (twice) and 50 mL of saturated brine, dried over Na$_2$SO$_4$, and concentrated under vacuum. The resulting residue was purified by silica gel flash chromatography.

**Method d** [1-(3-dimethylaminopropyl)-3-ethyl carbodiimide hydrochloride (EDC) coupling]. Various amines generated from method c (1 equiv) were added to a solution of individual short-chain fatty acids in dry THF (5−10 mmol/mL) under N$_2$, followed by the addition of EDC (1.3 equiv). After the solution was stirred overnight, THF was removed under vacuum, and the residue was dissolved in ethyl acetate (100 mL). The mixture was washed consecutively with 50 mL of water (twice) and 50 mL of saturated brine. The organic layer was dried over Na$_2$SO$_4$ and concentrated under vacuum. The resulting residue was purified by silica gel flash chromatography.

**Method e** (hydrogenolysis). The *N*-benzyloxy derivative resulting from method d was dissolved in 1:1 methanol/THF (5−10 mmol/mL), and 10% palladium on charcoal (10% w/w) was added. The mixture was treated with hydrogen under atmospheric pressure for 2 h and was filtered. The solvent was evaporated, and the residue was recrystallized with ethyl acetate.

**2,2,-Dimethyl-4-phenylbutyric acid.** Isobutyric acid (1.4 mL) was added dropwise to a mixture of diisopropylamine (2.2 mL, 0.015 mol) and 54% sodium hydride in mineral oil (0.74 g, 0.0165 mol) in THF (40 mL) and refluxed for 15 min. After the solution was cooled to 0 °C, a standard solution of *n*-butyllithium in heptane (1.45 mmol/mL; 9.4 mL) was added. After 20 min at 0 °C, the mixture was heated to 30−35 °C for 30 min. After the solution was cooled to 0 °C again, (2-bromoethyl)-benzene (2.8 mL, 15 mmol) was added to the reaction mixture over 20 min. The ice-bath was retained for 30 min, the mixture was then heated to 30−35 °C for 1 h, and then 40

mL of water was added to the reaction mixture at a temperature under 15 °C. The aqueous layer was separated, and the organic layer was washed with a mixture of 20 mL of water and 30 mL of ethyl ether. Aqueous layers were combined, back-extracted with 20 mL of ethyl ether, and acidified with 6 N hydrochloric acid, and the product was extracted with 30 mL of ethyl ether twice. The combined organic layer was washed with 20 mL of saturated brine, dried with Na$_2$SO$_4$, and concentrated under vacuum. Hexane was added to the resulting colorless oil to yield 1.1 g of white solid.

**Resolution of (±)-2-Isopropylphenylacetic Acid.** 2-Isopropylphenylacetic acid (2.3 g), (+)-$\alpha$-phenylethylamine (1.64 mL), and 63% aqueous ethanol (50 mL) were refluxed and allowed to cool slowly. The resulting salt was recrystallized four times from 63% aqueous ethanol. The salt was treated with 10% sulfuric acid at 0 °C, extracted with ethyl acetate, dried, and concentrated to yield 340 mg of (*R*)-(−)-2-isopropylphenylacetic acid, [$\alpha$]$^{25}_D$ −59.5° (CHCl$_3$, *c* 2.27). The mother liquids from the above four recrystalizations were combined, concentrated, acidified with 10% sulfuric acid at 0 °C, extracted with ethyl acetate, dried and concentrated, and then dissolved in 50 mL of ethyl alcohol. (−)-$\alpha$-Phenylethylamine (1.64 mL) was added to this solution. The process described above was repeated to obtain 320 mg of (*S*)-(+)-2-isopropylphenylacetic acid, [$\alpha$]$^{25}_D$ −59.5° (CHCl$_3$, *c* 2.13).

**HTPB:** $^1$H NMR (DMSO-$d_6$) $\delta$ 11.02 (s, 1H), 10.1 (s, 1H), 8.94 (s, 1H), 7.67 (m, 4H), 7.27 (m, 5H), 2.63 (t, *J* = 7.5 Hz, 2H), 2.35 (t, *J* = 7.4 Hz, 2H), 1.87 (m, 2H); HRMS exact mass of (M + Na)$^+$, 321.120961 amu; observed mass of (M + Na)$^+$, 321.11940 amu. Anal. (C$_{17}$H$_{18}$N$_2$O$_3$) C, H, N.

**4-Benzoylamino-*N*-hydroxybenzamide (1):** $^1$H NMR (DMSO-$d_6$) $\delta$ 11.1 (s, 1H), 10.51 (s, 1H), 8.97 (s, 1H), 7.85 (m, 4H), 7.61 (m, 5H); HRMS exact mass of (M + Na)$^+$, 279.074011 amu; observed mass of (M + Na)$^+$, 279.07370 amu. Anal. (C$_{14}$H$_{12}$N$_2$O$_3$) C, H, N.

**_N_-Hydroxy-4-(phenylacetylamino)benzamide (2):** $^1$H NMR (DMSO-$d_6$) $\delta$ 11.1 (s, 1H), 10.40 (s, 1H), 8.94 (s, 1H), 7.67 (m, 4H), 7.33 (m, 5H), 3.67 (s, 2H); HRMS exact mass of (M + Na)$^+$, 293.089661 amu; observed mass of (M + Na)$^+$, 293.08957 amu. Anal. (C$_{15}$H$_{14}$N$_2$O$_3$) C, H, N.

**_N_-Hydroxy-4-(3-phenylpropionylamino)-benzamide (3):** $^1$H NMR (DMSO-$d_6$) $\delta$ 11.09 (s, 1 H), 10.17 (s, 1H), 8.94 (s, 1H), 7.67 (m, 4H), 7.27 (m, 5H), 2.92 (t, *J* = 7.5 Hz, 2H), 2.63 (t, *J* = 7.4 Hz, 2H); HRMS exact mass of (M + Na)$^+$, 307.105311 amu; observed mass of (M + Na)$^+$, 321.10579 amu. Anal. (C$_{16}$H$_{16}$N$_2$O$_3$) C, H, N.

**_N_-Hydroxy-4-(5-phenylpentanoylamino)benzamide (4):** $^1$H NMR (DMSO-$d_6$) $\delta$ 11.04 (s, 1H), 10.14 (s, 1H), 8.94 (s, 1H), 7.67 (m, 4H), 7.27 (m, 5H), 2.51 (m, 4H), 1.61 (m, 4H); HRMS exact mass of (M + Na)$^+$, 321.120961 amu; observed mass of (M + Na)$^+$, 335.136611 amu. Anal. (C$_{18}$H$_{20}$N$_2$O$_3$) C, H, N.

**_N_-Hydroxy-4-[(4-phenylbutyrylamino)methyl]benzamide (5):** $^1$H NMR (DMSO-$d_6$) $\delta$ 11.2 (s, 1H), 9.0 (s, 1H), 8.4 (t, *J* = 5.8 Hz, 1H), 7.7 (d, *J* = 8.0 Hz, 2H), 7.21 (m, 7H), 4.3 (d, *J* = 5.8 Hz, 2H), 2.58 (t, *J* = 7.3 Hz, 2H), 2.18 (t, *J* = 7.3 Hz, 2H), 1.83 (m, 2H); HRMS exact mass of (M + Na)$^+$, 335.136611 amu; observed mass of (M + Na)$^+$, 335.13716 amu. Anal. (C$_{18}$H$_{20}$N$_2$O$_3$) C, H, N.

**[4-(2-Hydroxycarbamoylethyl)phenyl]-4-phenylbutyramide (6):** $^1$H NMR (DMSO-$d_6$) $\delta$ 10.36 (s, 1H), 9.80 (s, 1H), 8.70 (s, 1H), 7.52 (d, *J* = 8.5 Hz, 2H), 7.2−7.4 (m, 5H), 7.10 (d, *J* = 8.4 Hz, 2H), 2.75 (t, *J* = 7.4 Hz, 2H), 2.62 (t, *J* = 7.5 Hz, 2H), 2.15−2.4 (m, 4H), 1.8−2.0 (m, 2H); HRMS exact mass of (M + Na)$^+$, 349.152261 amu; observed mass of (M + Na)$^+$, 349.15223 amu. Anal. (C$_{19}$H$_{22}$N$_2$O$_3$) C, H, N.

**_N_-Hydroxy-4-[methyl(4-phenylbutyryl)amino]benzamide (7):** $^1$H NMR (DMSO-$d_6$) $\delta$ 11.18 (s, 1H), 9.11 (s, 1H), 7.80 (d, *J* = 7.5 Hz, 2H), 7.38 (d, *J* = 7.5 Hz, 2H), 7.21 (m, 5H), 3.18 (s, 3H), 2.48 (t, *J* = 7.5 Hz, 2H), 2.11 (t, *J* = 7.4 Hz, 2H), 1.78 (m, 2H); HRMS exact mass of (M + Na)$^+$, 335.136611 amu; observed mass of (M + Na)$^+$, 335.13859 amu. Anal. (C$_{18}$H$_{20}$N$_2$O$_3$) C, H, N.

**_N_-Hydroxy-4-(2-methyl-2-phenylpropionylamino)benzamide (8):** $^1$H NMR (DMSO-$d_6$) $\delta$ 11.05 (s, 1H), 9.34 (s, 1H),

8.93 (s, 1H), 7.68 (m, 4H), 7.28 (m, 5H), 3.33 (s, 6H); HRMS exact mass of $(M + Na)^+$, 321.120961 amu; observed mass of $(M + Na)^+$, 321.12255 amu. Anal. $(C_{17}H_{18}N_2O_3)$ C, H, N.

**4-(2,2-Dimethyl-4-phenylbutyrylamino)-*N*-hydroxybenzamide (9):** ^{1}H NMR (DMSO-$d_6$) δ 11.04 (s, 1H), 9.45 (s, 1H), 8.94 (s, 1H), 7.69 (m, 4H), 7.27 (m, 5H), 1.92 (m, 2H), 1.28 (s, 6H); HRMS exact mass of $(M + Na)^+$, 349.152261 amu; observed mass of $(M + Na)^+$, 349.15187 amu. Anal. $(C_{19}H_{22}N_2O_3)$ C, H, N.

**(*S*)-(+)-*N*-Hydroxy-4-(2-phenylbutyrylamino)benzamide [(*S*)-10]:** ^{1}H NMR (DMSO-$d_6$) δ 11.09 (s, 1H), 10.3 (s, 1H), 8.93 (s, 1H), 7.67 (m, 4H), 7.34 (m, 5H), 3.58 (t, *J* = 6.5 Hz, 2H), 2.10 (m, 1H), 1.74 (m, 1H), 1.18 (t, *J* = 7.3 Hz, 3H); $[\alpha]^{25}_D$ +91.1° (*c* 1.4, CH$_3$OH); HRMS exact mass of $(M + Na)^+$, 321.120961 amu; observed mass of $(M + Na)^+$, 321.11940 amu. Anal. $(C_{17}H_{18}N_2O_3)$ C, H, N.

**(*R*)-(−)-*N*-Hydroxy-4-(2-phenylbutyrylamino)benzamide [(*R*)-10]:** ^{1}H NMR (DMSO-$d_6$) δ 11.09 (s, 1H), 10.3 (s, 1H), 8.93 (s, 1H), 7.67 (m, 4H), 7.34 (m, 5H), 3.58 (t, *J* = 6.5 Hz, 2H), 2.10 (m, 1H), 1.74 (m, 1H), 1.18 (t, *J* = 7.3 Hz, 3H); $[\alpha]^{25}_D$ −90.9° (*c* 1.21, CH$_3$OH); HRMS exact mass of $(M + Na)^+$, 321.120961 amu; observed mass of $(M + Na)^+$, 321.11940 amu. Anal. $(C_{17}H_{18}N_2O_3)$ C, H, N.

**(*S*)-(+)-*N*-Hydroxy-4-(3-methyl-2-phenylbutyrylamino)-benzamide [(*S*)-11]:** ^{1}H NMR (DMSO-$d_6$) δ 11.09 (s, 1H), 10.3 (s, 1H), 8.93 (s, 1H), 7.67 (m, 4H), 7.34 (m, 5H), 2.38 (m, 1H), 1.74 (m, 1H), 1.03 (d, *J* = 6.5 Hz, 3H), 0.69 (d, *J* = 6.5 Hz, 3H); $[\alpha]^{25}_D$ +96.8° (*c* 1.0, CH$_3$OH); HRMS exact mass of $(M + Na)^+$, 335.136611 amu; observed mass of $(M + Na)^+$, 335.13710 amu. Anal. $(C_{18}H_{20}N_2O_3)$ C, H, N.

**(*R*)-(−)-*N*-Hydroxy-4-(3-methyl-2-phenyl-butyrylamino)-benzamide [(*R*)-11]:** ^{1}H NMR (DMSO-$d_6$) δ 11.09 (s, 1H), 10.3 (s, 1H), 8.93 (s, 1H), 7.67 (m, 4H), 7.34 (m, 5H), 2.38 (m, 1H), 1.74 (m, 1H), 1.03 (d, *J* = 6.5 Hz, 3H), 0.69 (d, *J* = 6.5 Hz, 3H); $[\alpha]^{25}_D$ −90.6° (*c* 1.0, CH$_3$OH); HRMS exact mass of $(M + Na)^+$, 335.136611 amu; observed mass of $(M + Na)^+$, 335.13604 amu. Anal. $(C_{18}H_{20}N_2O_3)$ C, H, N.

**In Vitro HDAC Assay.** HDAC activity was analyzed by using a HDAC assay kit (Upstate Biotechnology, Lake Placid, NY), following the manufacturer's instruction with slight modifications. This assay was based on the ability of DU-145 nuclear extract, which is rich in HDAC activity, to mediate the deacetylation of the biotinylated [3H]-acetyl histone H4 peptide that was bound to streptavidin agarose beads. The release of [3H]-acetate into the supernatant was measured to calculate the HDAC activity. Sodium butyrate (0.25−1 mM) was used as a positive control.

**Cell Viability Assay.** The effect of the test agents on cell viability was assessed by the 3-(4,5-dimethylthiazol-2-yl)-2,5-diphenyl-2*H*-tetrazolium bromide (MTT) assay in 96-well, flat-bottomed plates, in which 4,000 DU-145 cells/well were seeded. Cells were exposed to the test agent at the indicated concentrations in 10% FBS-supplemented RPMI 1640 medium at 37 °C in 5% CO$_2$ for the indicated time. The medium was removed and replaced by 150 μL of 0.5 mg/mL of MTT in RPMI 1640 medium, and the cells were incubated in the CO$_2$ incubator at 37 °C for 2 h. Supernatants were removed from the wells, and the reduced MTT dye was solubilized with 200 μL/well of DMSO. Absorbance was determined on a plate reader at 570 nm. Each treatment was repeated in six wells.

**Western Blot Analysis.** DU-145 cells $(1 \times 10^6)$ treated with the test agent at the indicated concentrations in 10% FBS-supplemented RPMI 1640 medium for 48 h were collected and sonicated. Protein concentrations of the lysates were determined by using a Bradford protein assay kit (Bio-Rad, Hercules, CA); equivalent amounts of proteins from each lysate were resolved in 10% SDS−polyacrylamide gel, and then transferred onto Immobilon−nitrocellulose membranes (Millipore, Bellerica, MA) in a semi-dry transfer cell. The transblotted membrane was washed twice with tris-buffered saline containing 0.1% Tween 20 (TBST). After being blocked with TBST containing 5% nonfat milk for 40 min, the membrane was incubated with the primary antibody (1:3000 dilution) in TBST/1% nonfat milk at 4 °C overnight. After treatment with the primary antibody, the membrane was washed three times with TBST for a total of 15 min, washed with goat anti-rabbit or anti-mouse IgG-horseradish peroxidase conjugates (diluted 1:3000) for 1 h at room temperature, and washed three more times with TBST for a total of 1 h. The immunoblots were visualized by enhanced chemiluminescence.

**Molecular Docking.** The crystal structure of HDLP in complex with TSA[10] was obtained from the Brookhaven Protein Data Bank (http://www.rcsb.org/pdb/; entry code, 1c3r), the A form structure of which was used in this study. The three-dimensional structures of small molecules were generated using the software SYBYL 6.9 (Tripos Associates, St. Louis, MO; 2002). Geiger charges were computed, and energy minimization was carried out with default parameters. The AutoDock Tools software (http://www.scripps.edu/pub/olson-web/doc/autodock/) was used to designate the rotatable bonds and generate grid parameter file and docking parameter file using a default parameter. Zinc ion was modeled by Amber force field potentials with parameters defined by Stone and Karplus ($r = 1.1$ Å, $\epsilon = 0.25$ kcal/mol) and a charge of +2.0 e as the initial parameters.[13] Docking was performed with AutoDock 3.05 (http://www.scripps.edu/pub/olson-web/doc/autodock/) which predicts the bound conformations of a small, flexible ligand to a nonflexible macromolecular target of known structure. This software is an automated docking package that combines a rapid grid-based method for energy evaluation with a Lamarckian genetic algorithm method for conformation searches.[14] The docked complexes for each inhibitor were selected according to the criteria of interaction energy in combination with geometrical matching quality. All of the molecular modeling calculations and manipulations were performed on Silicon Graphics O2 (Silicon Graphics Inc., Mountain View, CA).

## References

(1) Jenuwein, T.; Allis, C. D. Translating the histone code. *Science* **2001**, *293*, 1074−1080.
(2) Marks, P.; Rifkind, R. A.; Richon, V. M.; Breslow, R.; Miller, T.; Kelly, W. K. Histone deacetylases and cancer: causes and therapies. *Nat. Rev. Cancer* **2001**, *1*, 194−202.
(3) Marks, P. A.; Richon, V. M.; Rifkind, R. A. Histone deacetylase inhibitors: inducers of differentiation or apoptosis of transformed cells. *J. Natl. Cancer Inst.* **2000**, *92*, 1210−1216.
(4) Johnstone, R. W. Histone-deacetylase inhibitors: novel drugs for the treatment of cancer. *Nat. Rev. Drug Discovery* **2002**, *1*, 287−299.
(5) Jung, M. Inhibitors of histone deacetylase as new anticancer agents. *Curr. Med. Chem.* **2001**, *8*, 1505−1511.
(6) Grozinger, C. M.; Schreiber, S. L. Deacetylase enzymes: biological functions and the use of small-molecule inhibitors. *Chem. Biol.* **2002**, *9*, 3−16.
(7) Miller, T. A.; Witter, D. J.; Belvedere, S. Histone deacetylase inhibitors. *J. Med. Chem.* **2003**, *46*, 5097−5116.
(8) Rosato, R. R.; Grant, S. Histone deacetylase inhibitors in clinical development. *Expert Opin. Invest. Drugs* **2004**, *13*, 21−38.
(9) Marks, P. A.; Miller, T.; Richon, V. M. Histone deacetylases. *Curr. Opin. Pharmacol.* **2003**, *3*, 344−351.
(10) Finnin, M. S.; Donigian, J. R.; Cohen, A.; Richon, V. M.; Rifkind, R. A.; Marks, P. A.; Breslow, R.; Pavletich, N. P. Structures of a histone deacetylase homologue bound to the TSA and SAHA inhibitors. *Nature* **1999**, *401*, 188−193.
(11) Lu, Q.; Yang, Y. T.; Chen, C. S.; Davis, M.; Byrd, J. C.; Etherton, M.; Umar, A.; Chen, C. S. Zn$^{2+}$-chelating motif-tethered short-chain fatty acids as a novel class of histone deacetylase inhibitors. *J. Med. Chem.* **2004**, *47*, 467−474.
(12) Vanommeslaeghe, K.; Van Alsenoy, C.; De Profit, F.; Martins, J. C.; Tourwe, D.; Geerlings, P. Ab intio study of the binding of Trichostatin A (TSA) in the active site of histone deacetylase like protein (HDLP). *Org. Biomol. Chem.* **2003**, *1*, 2951−2957.
(13) Stote, R. H.; Karplus, M. Zinc binding in proteins and solution: a simple but accurate nonbonded representation. *Proteins: Struct., Funct., Genet.* **1995**, *23*, 12−31.
(14) Morris, G. M.; Goodsell, D. S.; Halliday, R. S.; Huey, R.; Hart, W. E.; Belew, R. K.; Olson, A. L. Automated docking using a Lamarckian genetic algorithm and empirical binding free energy function. *J. Comput. Chem.* **1998**, *19*, 1639−1662.